Send Orders for Reprints to reprints@benthamscience.net

Current Physical Chemistry, **2014**, *4*, 45-64

Theoretical Studies of Doped Solid Oxides for Fuel Cell Applications

J. G. Solano Canchaya[1,#,*] A. V. Gil Rebaza[2], D. S. Lemelle[1] and C. A. Taft[1]

[1]*Centro Brasileiro de Pesquisas Fisicas – CBPF, Rua Dr. Xavier Sigaud, 150 Urca, 22290-180, Rio de Janeiro Brasil;* [2]*Laboratorio de Ciencias de Superficies y Medio Porosos, Universidad Nacional de San Luis, Av. Ejercito de Los Andes # 950, San Luis – Argentina*

Abstract: Zirconia (ZrO_2) is of great importance as a support for systems where high ionic conductivity and mechanical stability are required. Doping/defects have a significant effect on the physical properties of this oxide by stabilizing the most symmetric phases, increasing the ionic conductivity and possible facilitating three phase interconnections in solid oxide fuel cells (SOFCs). Although Zirconia in its pure form exhibits different structures at high temperatures when it is alloyed with other oxides the high temperature cubic polymorph can be stabilized to temperatures low enough for fuel cell applications. Although there has been tremendous technological investment to obtain better materials, we are still far from an optimum solution. We start in this work with theoretical calculations as a support/participation in the search for more appropriate materials that will make this important technology viable in a wide range of applications in the near future. The calculations were performed in the framework of Density Functional (DFT) pseudopotential theory using the Projector Augmented Wave (PAW) with various approximations to the exchange-correlation functional. We investigate structural, electronic/band structure, density of states and charge densities for pure zirconia taking into consideration as well different dopants, their concentrations as well as vacancies for the various polymorphs with interest in fuel cell electrolyte applications.

Keywords: DFT, doping, fuel cells, zirconia.

INTRODUCTION

Due to the increasing energy demand there is a need for sustainable alternatives including solar and wind energies. Research towards storing technologies and eco-friendly highly efficient energy conversion is expanding exponentially worldwide. Fuel cells are electrochemical devices that allow the direct conversion of chemical into electrical energy (and heat) without involving the process of internal combustion and are not limited by the Carnot cycle. Their advantages include flexibility of operation for a wide range of applications, high efficiency, stationary and portable power supply, low pollutant emissions, continuous energy production, independence of efficiency from cell size, depending of course on that oxidant and fuel which are fed to the cell and the way they are reformed [1-11].

Each fuel cell is composed of a sequence of units, each with four components, the electrolyte, the electrode to the air (oxidant), the electrode for the fuel (hydrogen for example) and the interconnector. Nowadays, five major types of fuel cells can be distinguished by the type of electrolyte: alkaline fuel cells (AFCs, operational at ~ 80 ^{o}C), proton-exchange membrane fuel cells (PEMFCs, operational at ~ 60 – 80 ^{o}C), solid oxide fuel cells (SOFCs, initially at ~1000 ^{o}C,and more recently at 500 -600 ^{o}C), phosphoric acid fuel cells (PACFs, operational at ~180 ^{o}C) and molten carbonate fuel cells (MCFCs, 650 ^{o}C). The NASA Apollo space program in the 1950s started using AFC systems and this technology is still used for today`s shuttle missions [1-11].

Although there are different fuel cells technologies suited to their own materials and applications, they all share characteristics of no moving parts, high efficiency, quiet operation and low or zero emissions. The enormous potential markets include prime movers and/or auxiliary power units in vehicles, battery replacement in small portable electronic devices, residential combined heat and power (CHP), large-scale megawatt (MW) electrical power generation. Although the electrolyte is central, these fuel cells come in different arquitectures (tubular, planar,etc). The electrolytes can be liquid (molten salt or aqueous), solid (ceramic or polymer) with low electronic and high ionic conductivity. There may be oxide ion (SOFC), proton, carbonate or hydroxide conductors.

We find an electrode/catalyst at each side of the electrolyte whereas oxidant is given to the positive electrode (cathode) and to the negative electrode (anode) fuel is supplied. At the cathode, oxygen is reduced yielding O^{2-}, migrating through the electrolyte in order to react at the anode with the fuel liberating water if it is hydrogen. By connecting individual cells in series to form a `stack`, like in a battery, the voltage and power of the fuel cell are increased. Electrical interconnects can be used to join adjacent cells using flow channels as well to distribute reactants across the surface.

The low cell technologies (PEFCs, PAFCs and AFCs) require in general relatively pure hydrogen to maintain stable

*Address correspondence to this author at the Centro Brasileiro de Pesquisas Fisicas – CBPF, Rua Dr. Xavier Sigaud, 150 Urca, 22290-180, Rio de Janeiro Brasil; Tel/Fax: 55-21-2141-7201; E-mail: magnones6@hotmail.com

#Present address: Instituto de Física de Rosario (CONICET-UNR) Avenida Pellegrini 250, 2000, Rosario, Argentina.

1877-9476/14 $58.00+.00

performance and thus precious metal electrocatalysts which can be deactivated by carbon monoxide at the low operating temperatures. If hydrocarbons are used for fuel, a processor will be required adding to the cost and complexity of the system and eroding the efficiency. The PEFCs and SOFCs are currently attracting most attention and budgets [1-11].

Consequently, there has been a dramatic world wide interest increase over the last ~ 20 years in solid oxide fuel cells (SOFCs). The joint effort of Government, Private Industry, Educational institutions and National laboratories is pushing research development towards high efficiency, fuel flexible SOFCs for stationary market large central power plants as well as the transportation sector.

SOFCs, among the different type of fuel cells, provide significant environmental benefits and offer additional advantages, such the possibility of exploiting a wide range of applications with fuel flexibility allowing a variety of hydrocarbons to be utilized (including renewable fuels from biomasses). It can run on CO, H_2, H_2/CO-rich reformate gases as well as gasified liquid hydrocarbons whereas the need for external reformers can be eliminated.

The SOFC anode/fuel electrode is a multi-functional component. It is responsible for the establishment of the electro motoric force, and should be catalytically active towards reforming and shift reactions and unwanted side reactions such as coke formation or self-oxidation (corrosion). Oxygen ions are delivered by the solid electrolyte phase. The reactants are delivered by the gas phase and takes up products as well. The solid electrode phase takes up electrons. We have the concept of a three-phase boundary (TPB): electrochemistry can only take place in locations where all three components are spatially close to each other. The SOFC anodes are designed to have a high volumetric TPB length connected to percolating transport pathways for electrons, ions and gaseous species [1-11].

In order to avoid ohmic losses the current SOFC technology based a lot on stabilized zirconia electrolytes requires the cell to operate in the 800 -1000 ^{o}C range. The high operating temperatures are the main cause for the still limited SOFC commercialization, since they require usage of expensive materials for interconnectors, large energy input to heat the cell up to the operating temperature, long start-uptime.

ZrO_2 (group IV-B oxides) is a ceramic material with great potential for the development of solid oxide fuel cell electrolytes. At ambient conditions zirconia stabilizes in the monoclinic phase whereas at ambient pressure and temperatures above 1400 K transforms to the tetragonal phase. At temperatures of ~ 2570 K it transforms into a cubic fluorite structure. The requisites for a ceramic to act as a solid electrolyte is that it has a concentration of ionic defects nearly 1000 times superior to the electronic defects. Thus the solid electrolyte ceramic is a pure solid (intrinsic conductor) with an energy gap superior to 3 eV or a solid solution where the number of ionic defects has been increased by the formation of solid solutions (extrinsic conductors) [12-15].

For these ceramic materials with the fluorite structure the ionic conduction is determined by the oxygen vacancies. Among these materials one of the most studied for usage as fuel cells of oxide is Zirconia stabilized with Yttria (YSZ), in which the substitution of Z^{4+} by Y^{3+} yields vacancies for ionic conductivity. Other ceramics based on zirconia also have higher ionic conductivities such as zirconia stabilized with Ca (CaO) and Sc (Sc_2O_3).

There is a need to better understand the mechanisms of fuel oxidation and side reactions in SOFC anodes, developing materials to produce reasonable power output at intermediate temperatures (400-700 ^{o}C) yield more reliable sealing, cheaper interconnects, decrease in thermal expansion, rapid start-up and negligible electrode sintering. Reduction of initial and operational costs may yield important application in new fields. This is however not straightforward since at the cathode and anode, the chemical reactions as well as the ion transport in the electrolytes are thermally activated. Scientists are decreasing thickness (ohmic losses) or usage of other materials. YSZ has insufficient ionic conductivity to function as the electrolyte for intermediate or low-temperature SOFC. Sc stabilized zirconia indicates the highest oxide ionic conductivity in zirconia based systems. However the ionic conductivity decreases during aging at high temperatures and there is a drastic degradation of electrical and mechanical properties with aging at relatively low temperatures in both YSZ and ScSZ.

There is thus an intensive search for novel chemically stable and highly conductive electrolyte materials, i.e there is currently significant effort to raise the operating temperature of PEFCs and reduce that of SOFCs for a range of applications[1-11].

Transport and reactions are thermally activated and resistance can be lowered by using alternative materials or by decreasing thickness/ohmic losses. Doped lanthanum, ceria, galate and bismuth are examples of conducting electrolytes. However, there has been increasing interest in proton-conducting ceramics such as perovskites which when exposed to water vapor atmospheres or hydrogen indicates good proton conductivity and smaller values of activation energy [1-11].

The objective of this work is the theoretical study (Periodic Density functional pseudopotential theory using the projector augmented wave method [16-25] of the pure, defective (vacancies) and doped (Ca, Sc) ceramic oxides (cubic, tetragonal, monoclinic polymorphs) such as ZrO_2, i.e the physical-chemical processes that take place at the metal-oxide surfaces from first principles, i.e making a structural, and electronic/band structure, charge and density of states investigation of the surfaces with dopants and vacancies in different crystallographic directions and vacancies taking into consideration their importance in fuel cells.

THEORETICAL METHODS

There are many polymorphic structures of ZrO_2 in different intervals of temperature and pressure. At atmospheric pressure there are 3 stable polymorphic structures, i.e the monoclinic phase (m-ZrO_2), C^5_{2h} which is stable at low temperatures (from room temperature to 1170 ^{o}C), the tetragonal phase (t-ZrO_2), D^{15}_{4h} which is stable between 1170 ^{o}C and 2370 ^{o}C; the cubic phase (c-ZrO_2), which is called fluorite, and is stable between 2370 and 2680 ^{o}C. At

high pressures, many phase transitions have been observed experimentally. These intermediary orthorhombic structures which only exist at high pressures are considered derivatives of the monoclinic and tetragonal structures among which we have Ortho-I,which can be found between 3 and 5 GPa, Ortho-II which can be found between 22 and 27 GPa and Ortho-III which is observed between 37.5 and 42.5 GPa [12-15].

The characteristics of the 3 phases observed at atmospheric pressure are the fluorite structure F_{m3m}, which is described by the primitive cell containing 3 atoms (one Zr and two O), is a structure composed of a sub-network of cubic cations, centralized in the faces (FCC closed-Packed) where all the tetrahedral sites are occupied by anions (O). The tetragonal structure of zircônia is described by 3 structural parameters. The first 2 are given by the parameter a specifying the unit cell in the spatial directions x and y, and the parameter c yielding the direction z. The third parameter describes the change in internal structure related to dislocation of the oxygen from the ideal positions (separating from the symmetry of the cubic phase of fluorite) since at the tetragonal phase of zirconia there is an internal dislocation of the atoms of oxygen towards the z direction, i.e the oxygen atoms of neighboring columns are dislocated alternatively up and downwards by the distance Δc. Thus the last parameter called dz describes the dislocation relative to the oxygen atoms given by dz =Δc/c. The monoclinic structure is considered a variant of the fluorite structure. In this arrangement the Zr atoms exhibit lower coordination where the form of the polyhedron of coordination indicates two types of oxygen with different coordination O_1 with a coordination of 3 and O_2 with a coordination of 4.

In this work we investigate solid solutions of ZrO_2-CaO and ZrO_2-Sc_2O_3 concentrations of 12.5%, 25% and 14%, 33% mol of CaO and Sc_2O_3 distributed periodically in their respective supercells.

The calculations are performed using the Vienna ab initio simulation package VASP which is a density-functional-theory (DFT) code, working in a plane-wave basis set. Electron-ion interactions are described using the projector augmented wave method (PAW) with plane waves up to an energy cufoff (E_{cut}). Ultrasoft pseudopotentials of Vanderbilt (USPP) are used. For exchange and correlation functionals we use the local density approximaton (LDA) with the functional of Ceperly-Alder (CA), as well as the GGA functionals of Perdew *et al* (PW91), and that of Perdew-Burke-Ernzerhof (PBE). We note that other revised DFT functionals are available in the literature [16-25]. We use an electronic configuration of Zr with 10 electrons ($5s^14d^35p^6$) and O with 6 electrons ($2s^24p^4$).

The integration over the first Brillouin zone is done over a lattice of k-points using the Monkhorst-Pack method. The calculations were done with different choices, yielding the k-points to produce converging results. We take into consideration that the geometrical optimization is ended when the difference of energies between the two successive iterations is small.

Extensive calculations were done to determine the cutoff energies (E_{cutoff}) and the quantity of k points to obtain convergent results. Using USPP with LDA and GGA the values of 400eV for the cut energy and the choice of a k-mesh of 9x9x9 k points in the Monhkhorst-Pack scheme. In the method of PAW with the approximation PBE using 500 eV as cut energy, a k-mesh of 11x11x11 is sufficient to describe the crystals to the desired approximation. In all cases the optimization of the geometrical cell parameters was varied as a function of total energy in order to find the optimized parameters.

Thus the parameter a was optimized whereas the form of the cell and the atomic positions were maintained constant with the criteria that the cell parameter is that which minimizes the total energy. The internal parameters were relaxed using an algorithm of conjugated gradient whereas the cell and it's atomic positions were relaxed. The form of the cell and atomic positions were relaxed until the forces on the atoms were less than 0.02 eV/A. The tetragonal structure is defined by 3 parameters where the first two are experimental. As mentioned previously the position z of the oxygen atoms along the z azis is described by the adimensional parameter dz assim z = (0.25 + dz) × c. The cell parameter is investigated with respect to the total energy whereas the ratio b/a and c/a are maintained constant at the experimental value.

We also calculated the total density of states and by orbital, the band structure and the density of charge in 2d cuts in the direction (001). We then calculated the energetic jump (E_{gap}) between the occupied and virtual states. This value is calculated as the difference between the energies between the first virtual state and the energy of the first occupied state.

In this work we investigate solid solutions of ZrO_2-CaO and ZrO_2-Sc_2O_3, concentrations of 12.5%, 25% and 14%, 33% mol of CaO and Sc_2O_3 respectively distributed periodically in their respective supercells. Dopants as well as nearest and next nearest oxygen vacancies to dopants are simulated.

RESULTS AND DISCUSSION

In Figs. (**1-12**) we give total and partial density of states, band structure, charge densities for the cubic, tetragonal and monoclinic phases of ZrO_2 using, USPP, PAW and exchange correlations. Pseudopotentials are introduced to avoid the need for an explicit treatment of the strongly bound and chemically inert core electrons. In Ultrasoft potentials the norm-conservation criteria is dropped, but the logarithmic derivatives are matched at two or more reference energies spanning the entire range of eigenvalues of the valence electrons. The LDA used is based on Quantum Monte-Carlo simulations for the homogeneous electron gas. The ultrasoft pseudopotentials have the merit to make calculations for first row elements and for systems with d or f-electrons feasible at tractable effort. The PAW method represents an attempt to achieve simultaneously the computational efficiency of the pseudopotential method as well as the accuracy of the full-potential linearized augmented-plane-wave (FLAPW). It correctly describes the nodal features of the valence orbitals which are also correctly orthogonalized to the core wave functions. The PW91 functional has been constructed using

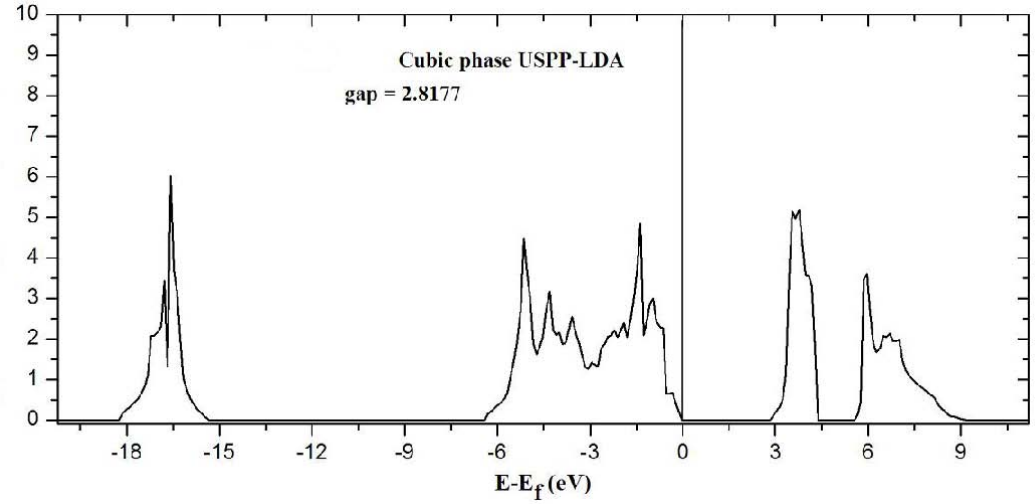
Cubic phase USPP-LDA
gap = 2.8177
E-E$_f$ (eV)

(A)

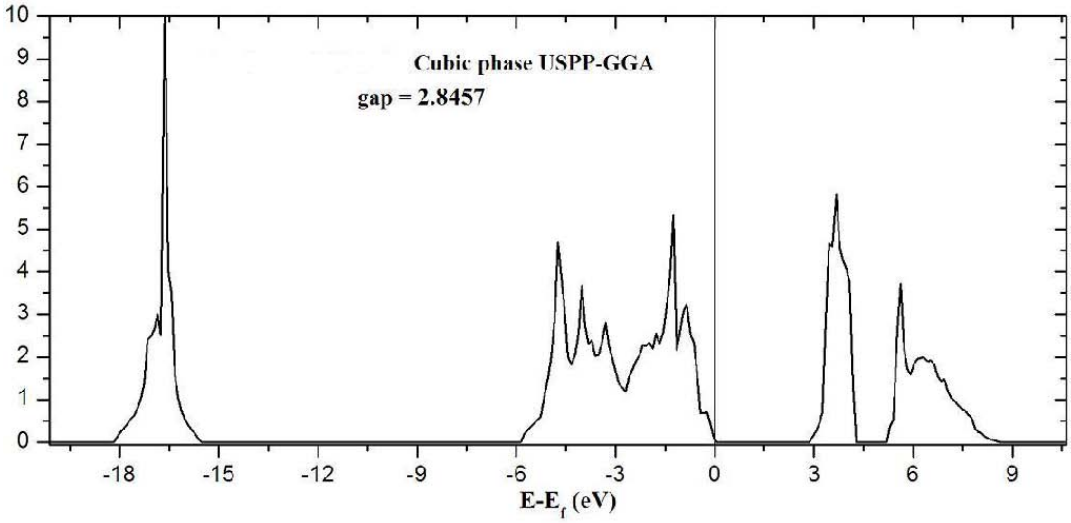
Cubic phase USPP-GGA
gap = 2.8457
E-E$_f$ (eV)

(B)

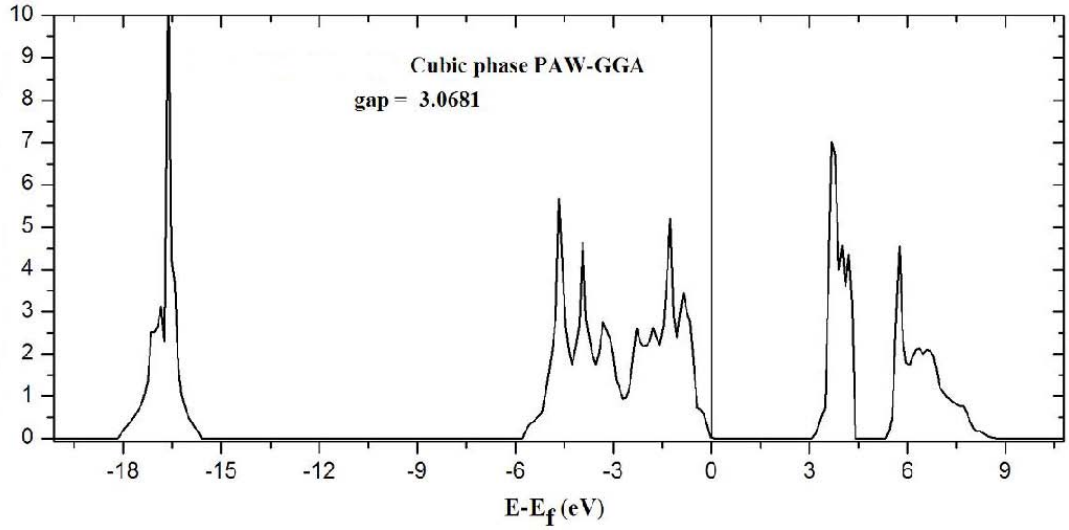
Cubic phase PAW-GGA
gap = 3.0681
E-E$_f$ (eV)

(C)

Fig. (1). contd….

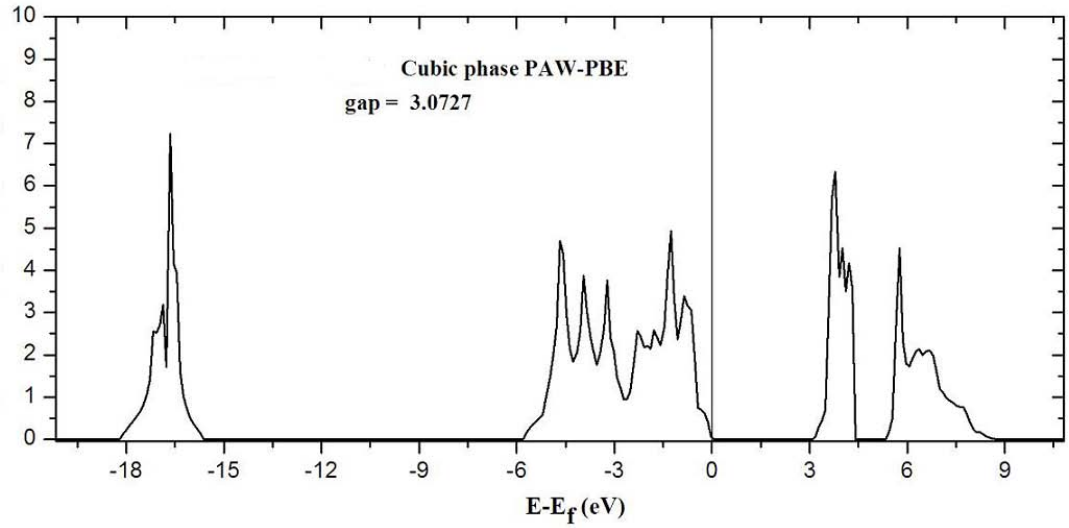

(D)

Fig. (1). Total Density of states for the cubic phase (**a**, **b**, **c**, **d**) USPP-LDA, USPP-GGA(CA), PAW-GGA(CA) and PAW-PBE respectively. All the energies are given with respect to the Fermi Energy.

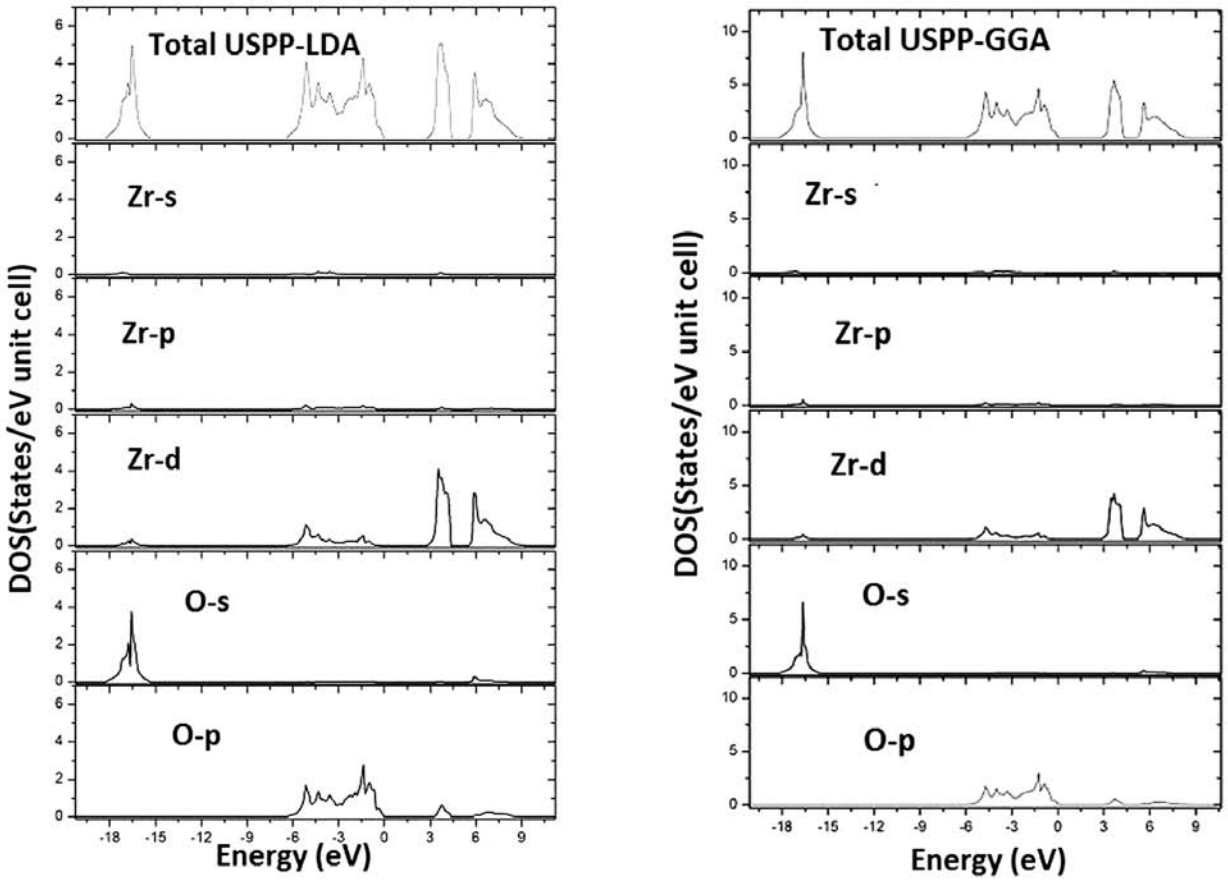

(a) **(b)**

Fig. (2). Density of states per orbital for the cubic phase for USPP-LDA, (b) USPP-LDA and USPP- GGA(CA). All energies are given with respect to the Fermi Energy Ef.

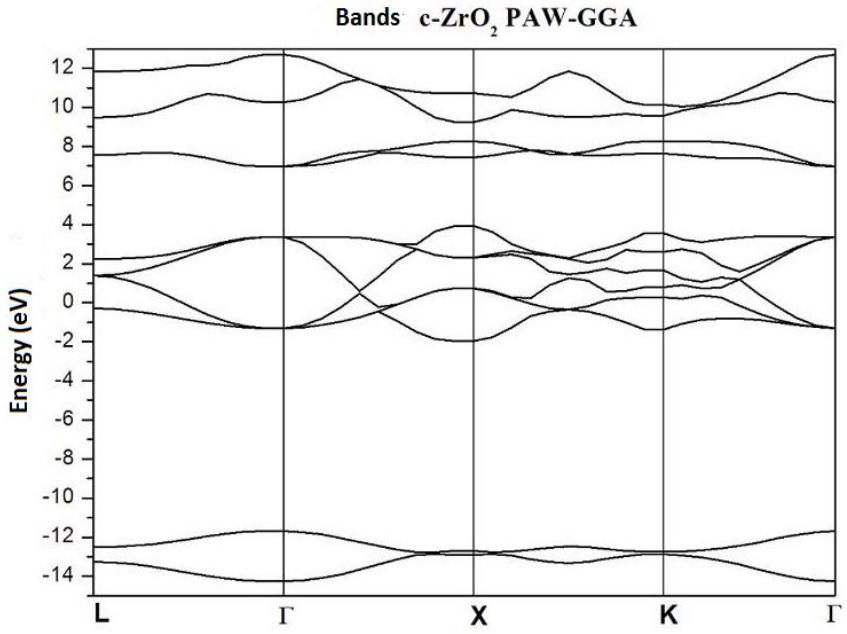

Fig. (3). Diagram of electronic bands for the cubic phase for (a) PAW-GGA (CA).

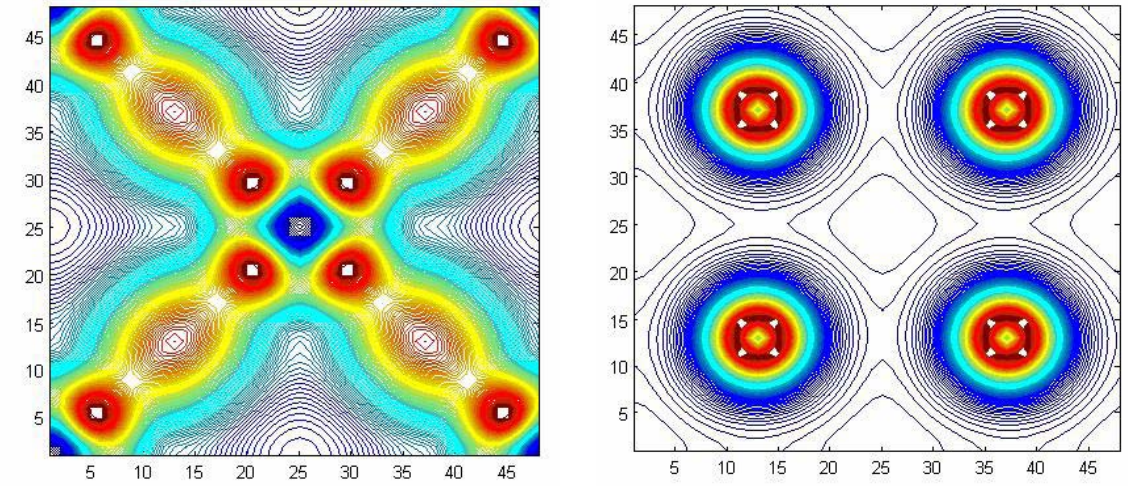

Fig. (4). Charge Density in the direction (001) of the unit cell of c-ZrO2 para (**a**, **b**) USPP-GGA and (c,d)PAW-GGA(CA).

QMC data for the uniform electron gas and exact properties of the exchange-correlation hole. PBE presents a more elegant derivation of the functional using exact properties of the exchange-correlation energy. GGA corrects the over-binding tendency inherent in the LDA, with a certain tendency to overcorrect: lattice constants are on average underestimated, PBE overestimates them by nearly the same amount.

For the case of doping with calcium the cut-off cinetic energy used is 500 eV with a number of K points of 9x9x9. A kinetic energy cut of 550 eV and a number k-points of 5x9x9 are sufficient to obtain a differential in energy of 0.01 eV/atom. In all cases we did an optimization of cell parameters and geometries. We also relaxed the atomic positions using the conjugated gradient algorithm (CG) that accompanies the changes until the forces on the atoms are less than 0.02 eV/A.

The total and angular decomposition of the density of states (DOS) for the cubic phase (Figs. **1**, **2**) indicates that the top of the valence band is formed by orbitals of the type O-2p whereas the core states are formed by O-2s and Zr-4p. For the tetragonal phase (Figs. **5**, **6**) the first states are Zr 4s and 4p followed by the O-2s states. The oxygen p band which is the highest occupied energy band is totally filled by transfer of Zr-d electrons to each O oxygen ion, the conduction band is formed mainly by Zr-d orbitals. A similar

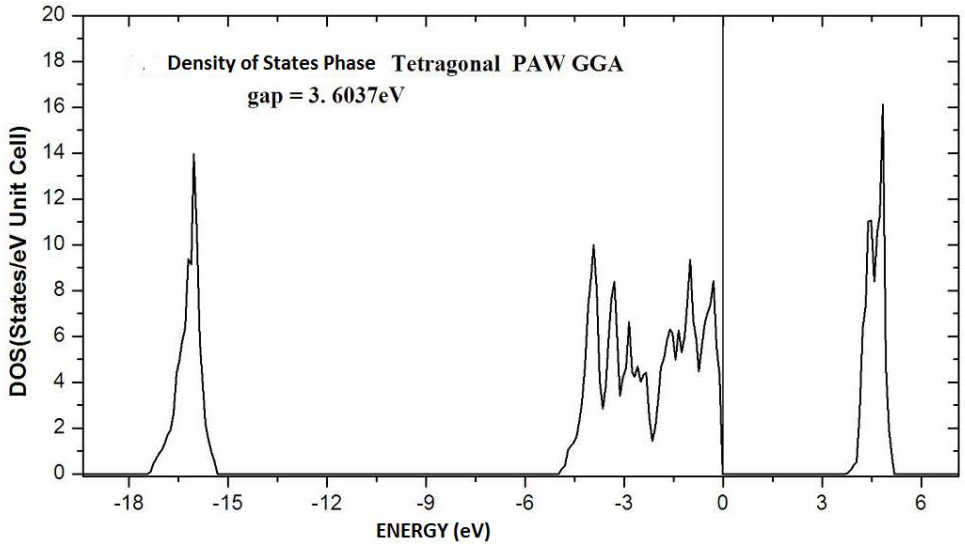

Fig. (5). Total density of states for the tetragonal phase of ZrO2 PAW-GGA (CA). All the energies are given with respect to the Fermi energy Ef.

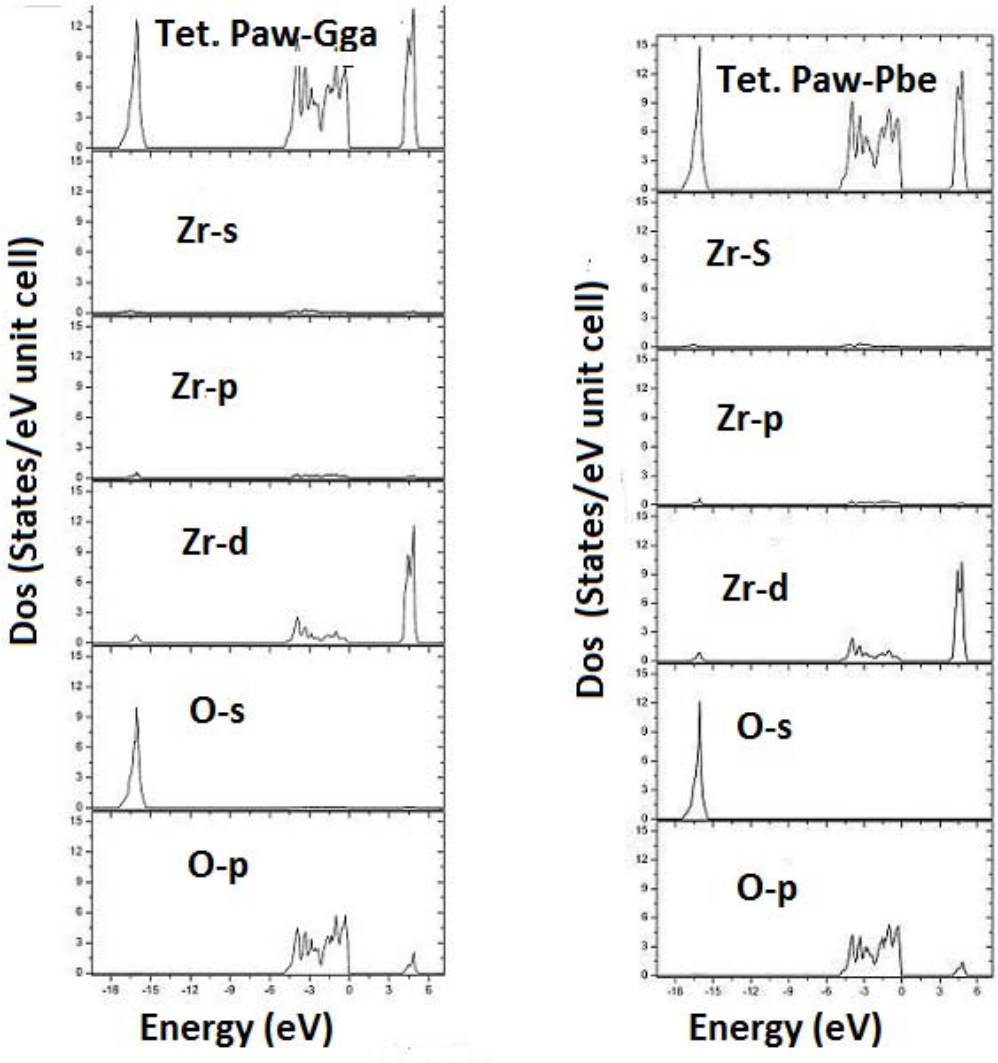

Fig. (6). Total density of states per orbital for the tetragonal phase for ZrO2 PAW-GGA(CA)and PAW-PBE. All the energies are given with respect to the Fermi Ef;

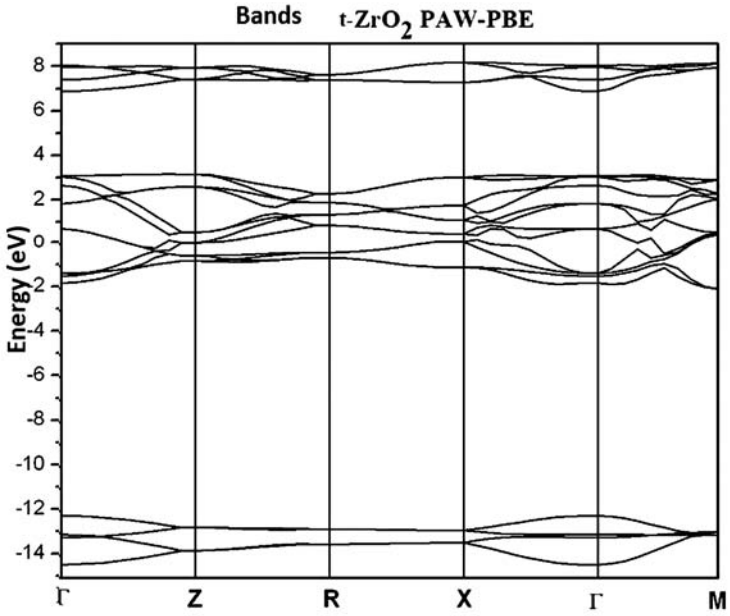

Fig. (7). Diagram of electronic bands for the tetragonal phase of ZrO2 PAW-PBE.

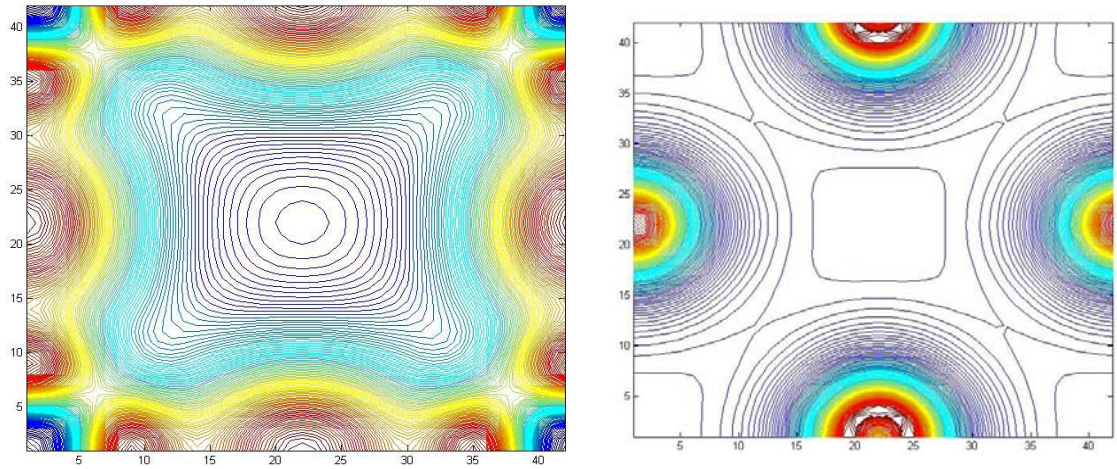

Fig. (8). Charge density for the tetragonal phase of ZrO2 PAW-GGA (CA). All the energies are given with respect to the Fermi energy Ef.

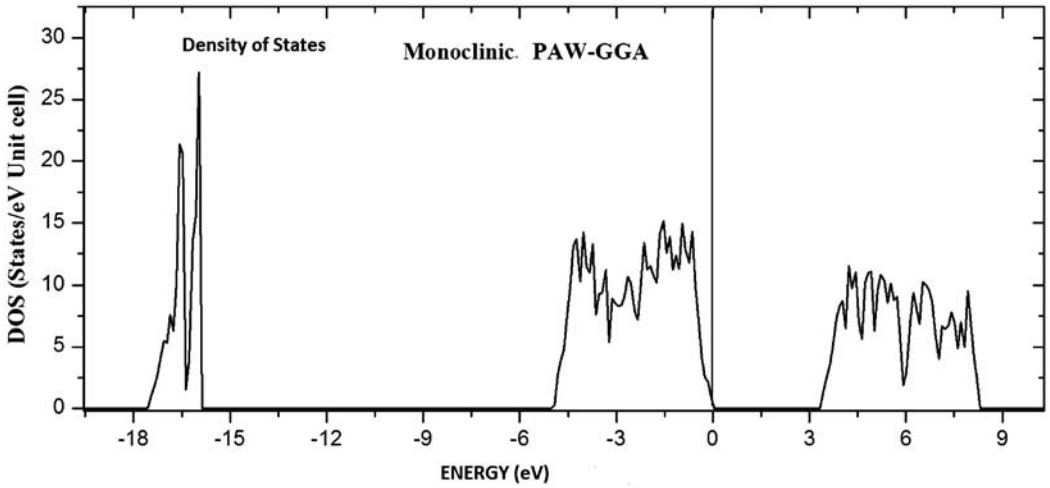

Fig. (9). Total density of states for the monoclinic phase of ZrO2 PAW-GGA (CA). All the energies are given with respect to the Fermi energy Ef.

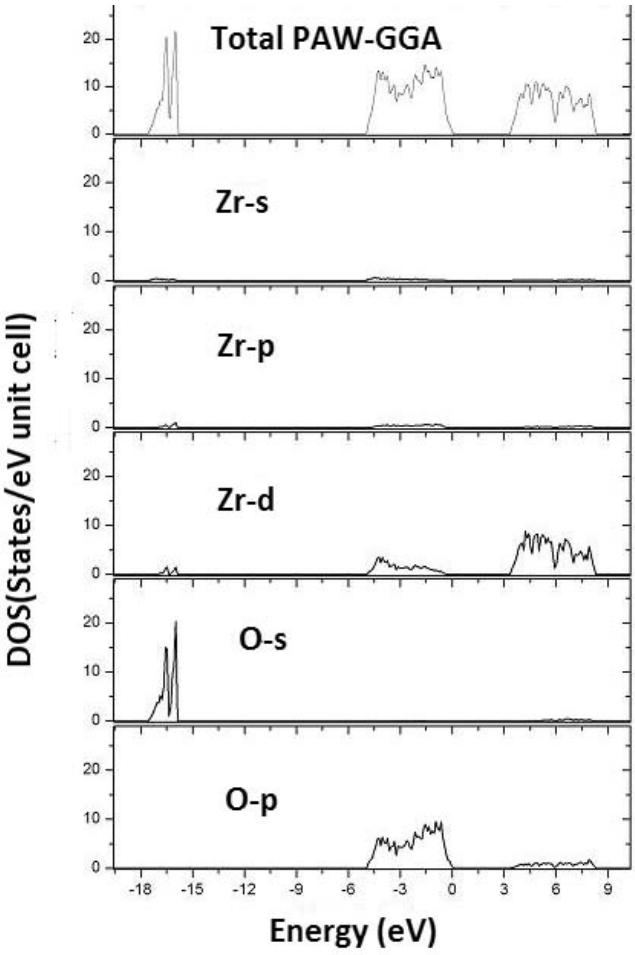

Fig. (10). Total density of states per orbital for the monoclinic phase for ZrO2 PAW- GGA (CA)and PAW-PBE. All the energies are given with respect to the Fermi Ef;

behavior was obtained for the DOS of the monoclinic phase (Figs. **9**, **10**) containing a valence oxygen band O-2s and 2p as well as a conduction band of Zr 4d. There should be a transfer of electrons from Zr-5s and Zr-4d to the oxygen atoms of the crystal. As we lower the symmetry we should find more Zr 4d and O 2p orbital σ and π hybridization bonding in the valence band as well as Zr and p antibonding in the conduction band.

Effectively, from the DOS and charge densities (Figs. **4**, **8**, **12**) it is possible to observe the formation of hybrid orbitals and an increase of the charge density between Zr and O atoms as we reduce the symmetry of the structures. There is a general tendency to increase the Zr(d) population, i.e an increase in the Zr-O overlap population as we go to lower symmetries such as the tetragonal and the monoclinic phase. We can also appreciate that this increase of covalency favors structures with a lower coordination number which is appreciated in the polymorphic structures i.e the coordination decrease from a coordination of 8 for Zr in the fluorite structure to a coordination or 7 in the monoclinic passing through an intermediate value in the tetragonal phase. Thus the covalent bond between Zr-O is one of the factors that influence the stability of the less symmetric phases and lower coordination of ZrO_2.

In Figs. (**3**, **7**, **11**) we give the band gaps for the cubic, tetragonal and monoclinic phases of pure Zirconia using different combination of methods. The band gaps are indirect. They are also above 3 eV which is required for ion conductors in SOFCs electrolytes. There are no states in the band gap. The calculated results are all smaller than the experiment data (depending on crystal phase and method of determination) of 4.2 to 6.1 eV [27-29] due to the well-known underestimation of conduction band state energies in DFT calculations. GGA functions underestimate the band gap which is remedied at higher levels of theory. Screened exchange (sX), weighted density approximation (WDA), hybrid functionals (HSEO6, PBEO, B3LYP), weighted density approximation (WDA), DFT+U, yield gaps values closer to experimental ones [30-33]. These models require greater computational effort and are not always feasible of extensive sampling and large models.

The calculated charge densities (Figs. **4**, **8**, **12**) also support the formation of hybrid orbitals and an increase in the charge density between the atoms of Zr and O with a reduction of the symmetry of the structures, i.e the covalent type bond between the Zr-O should be one of the factors that influence the stability of the phases of lower symmetry and lower coordination numbers in ZrO_2.

We investigate solid solutions of ZrO_2-CaO and ZrO_2-Sc_2O_3, with concentrations of 12.5%, 14%, 25% and 33% mol of CaO and Sc_2O_3 respectively distributed periodically in their respective supercells. Our calculations included PAW and PBE.

Calculations were made to find the cut in kinetic energies (E_{cutoff} and the number of k- points to obtain convergent results. For the case of doping with calcium the cut-off cinetic energy is 500 eV with a number of K points of 9x9x9. A kinetic energy cut of 550 eV and a number K-points of 5x9x9 are sufficient to obtain a differential in energy of 0.01 eV/atom. In all cases we did an optimization of cell parameters and geometries. We also relaxed the atomic positions using the conjugated gradient algorithm (CG) that accompanies the changes until the forces on the atoms are less than 0.02 eV/A.

We start with the investigation of Zirconia doped with cations such as Ca^{2+}, which follows the stoichiometry shown in the Fig. (**13a**) where we include explicitly the Ca dopant and it`s nearest neighbor (NN) vacancy. In Fig. (**13b**) we explicitly include Ca as well as both nearest neighbor (NN) and next nearest neighbors (NNN) oxygen vacancies with respect to dopant Ca^{2+}.

Fig. (**14a**) indicates the total density of states for solid solutions with 25% mol of CaO. Fig. (**14b**) indicates the total density of states for the solid solutions with 12.5 % mol of CaO with a NN vacancy with respect to the dopant. Fig. (**14c**) shows the total density of states with 12.5% mol of CaO and vacancy NNN to dopant.

In Fig. (**14d**) we indicate the partial density of states per orbital using 25% mol CaO whereas in Fig. (**14e**) at 12.5% mol CaO we also include NN oxygen vacancy with respect to the dopant. In Fig. (**14f**) we use 12.5% mol Ca concentration including NNN oxygen vacancy with respect to the dopant. Again we note that the explicit inclusion of

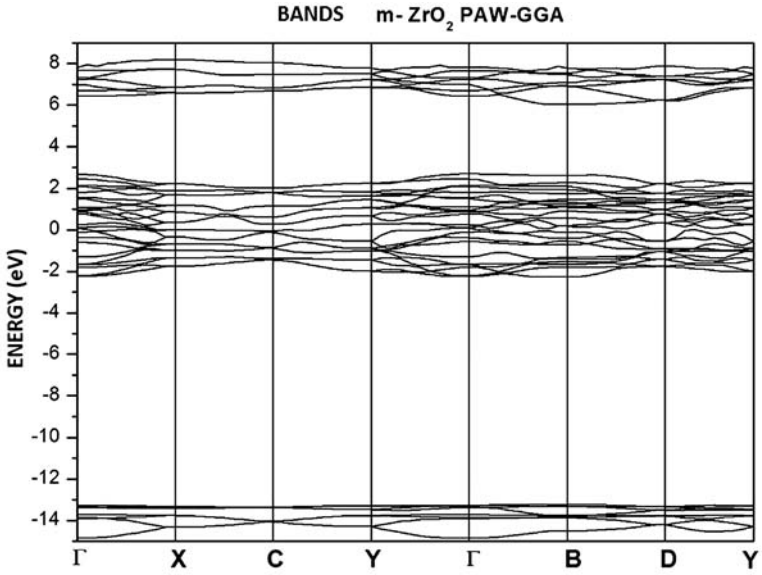

Fig. (11). Diagram of electronic bands for the monoclinic phase of ZrO2 PAW-GGA (CA).

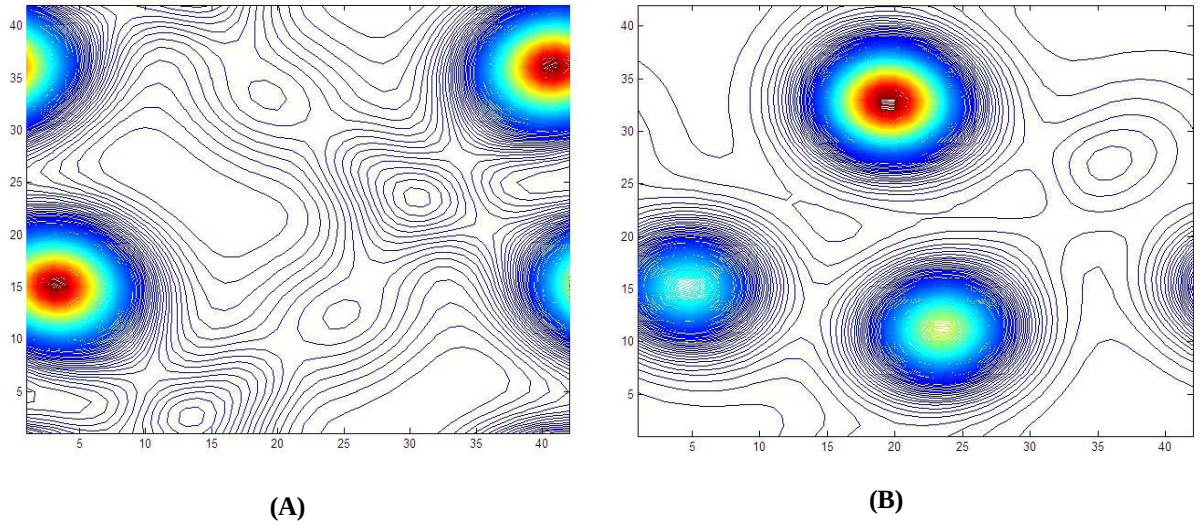

(A) **(B)**

Fig. (12). Charge density for the monoclinic phase of ZrO2 PAW-PBE. All the energies are given with respect to the Fermi energy Ef.

vacancies and dopants include new Ca-s and Ca-p states in the valence and conduction bands but not in the band gaps.

From the partial density of states per orbital of the doped Ca system it is possible to observe that for a concentration of CaO of 25% mol the deeper bands are composed mostly of O-2s character and the top of the valence band is composed mainly of orbitals of the type O-2p with a small Zr-4d contribution. The conduction band is formed mainly of orbitals Zr-4d. In the case of the doping of calcium with 12.5% the character of the top of the valence band does not change whereas the conduction bands are formed mostly by Zr-4d orbitals.

For doping with 25% mol CaO Fig. (**15**) indicates the charge density in the (100) direction of the unit cell. Fig. (**15a**) indicates the layer of the Ca dopant and Zr neighbors. Fig. (**15b**) indicates the oxygen vacancy and consequent reorganization of the oxygens. Fig. (**15c**) shows the new arrangement of Zr and oxygens. There is a preference for covalent bonding of oxygens with Zr whereas the Ca bonds are mostly ionic. Fig. (**15d**) indicates the new re-organization of oxygens, i.e migration of vacancies and oxygens (allowing ionic conductivity).

For doping with 12.5% mol CaO Fig. (**16**) indicates the charge density in the (100) direction of the unit cell containing a NN vacancy with respect to the dopant. Fig. (**16a**) indicates the layer where we find Zr. Fig. (**16b**) indicates the oxygen vacancy and new arrangement of oxygens, Fig. (**16c**) indicates the layer where we find dopant Ca. Fig. (**16d**) indicates the new arrangements of the oxygens. Covalent Zr-O bonds, ionic CaO bonds, oxygen migration (ionic conductivity) is suggested.

For doping with 25% mol CaO and including a NNN relative to dopant CA, Fig. (**17**) indicates the charge density in the (100) direction of the unit cell. Fig. (**17a**) indicates the

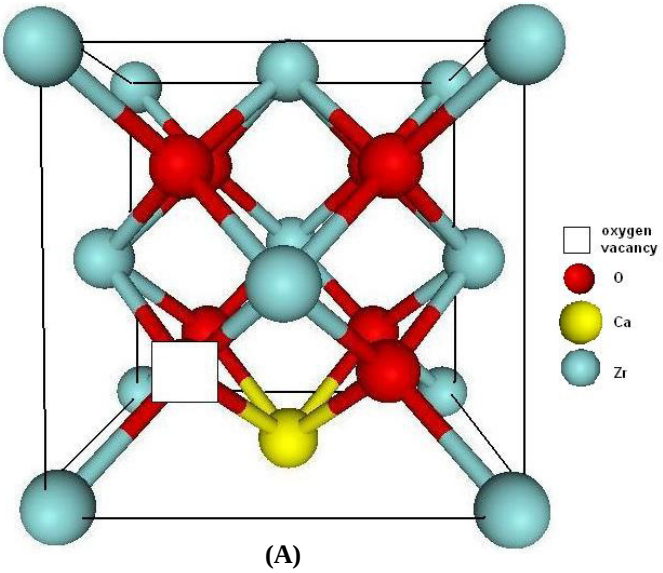

(A)

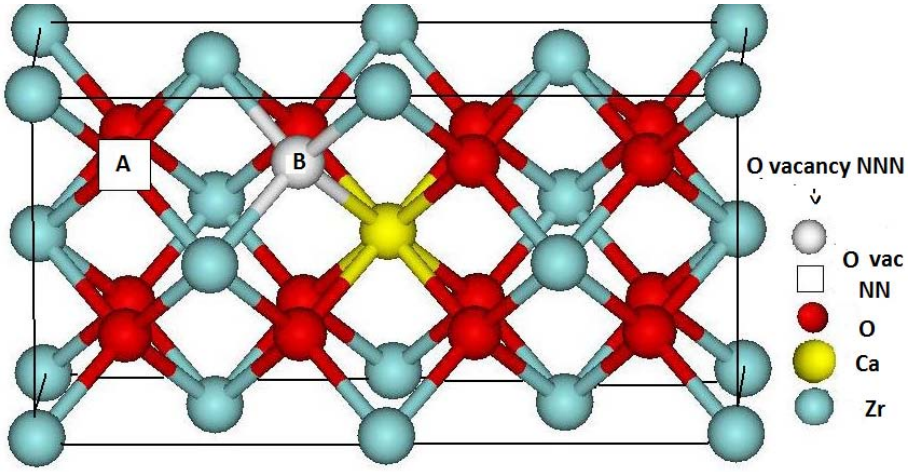

(B)

Fig. (13). (**a**) Unit cells for the solid solutions with 25% mol CaO. (**b**) Unit cell for the solid solution with 12.5 % mol CaO where □ (blank) indicates the oxygen vacancy in a position NNN as well as NN with respect to the position of the calcium dopant atom Ca.

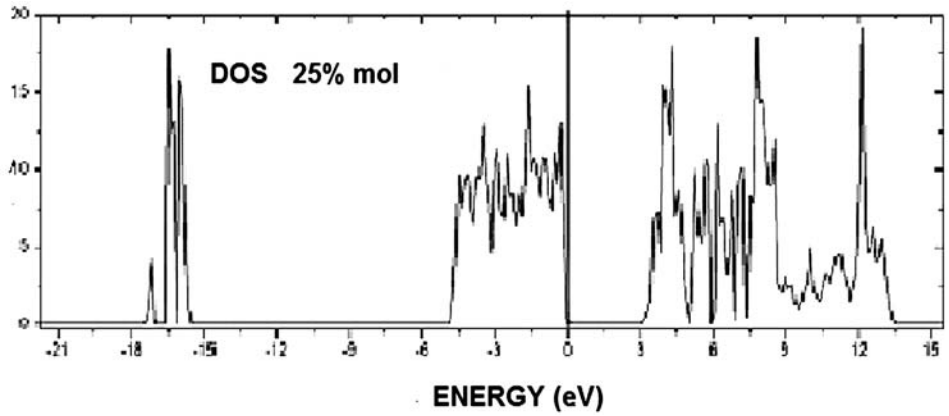

(A)

Fig. (14). contd….

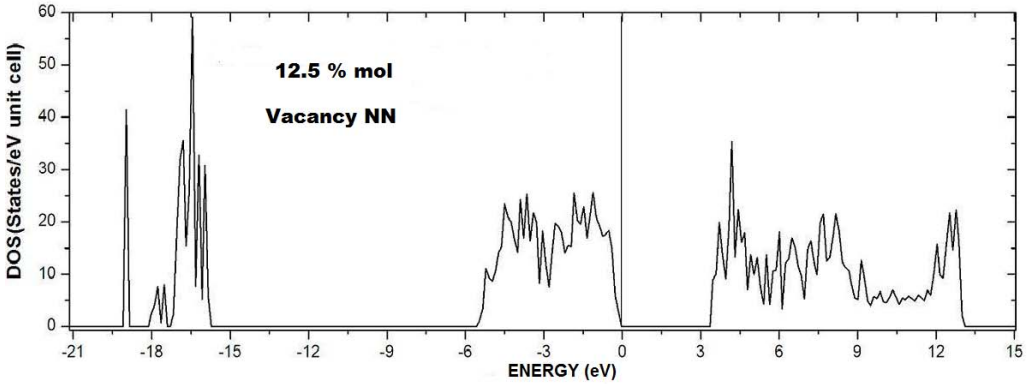

(B)

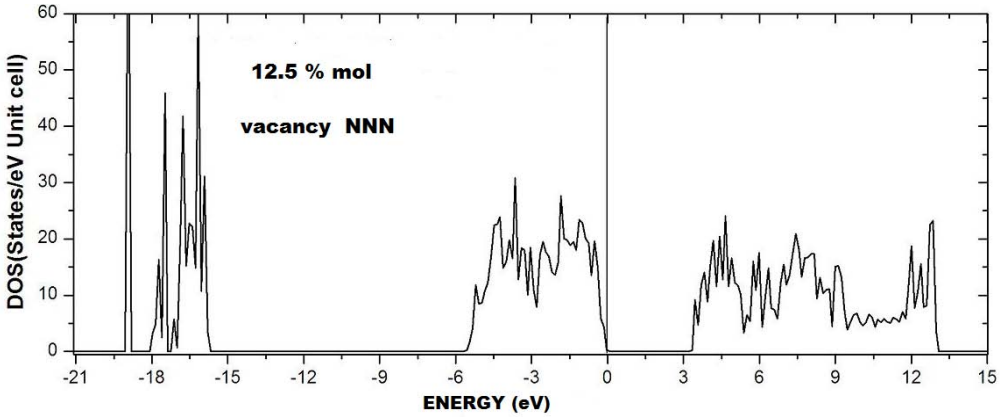

(C)

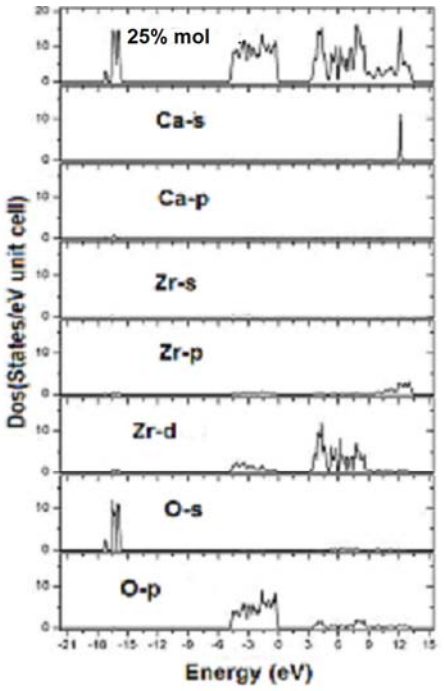

(D)

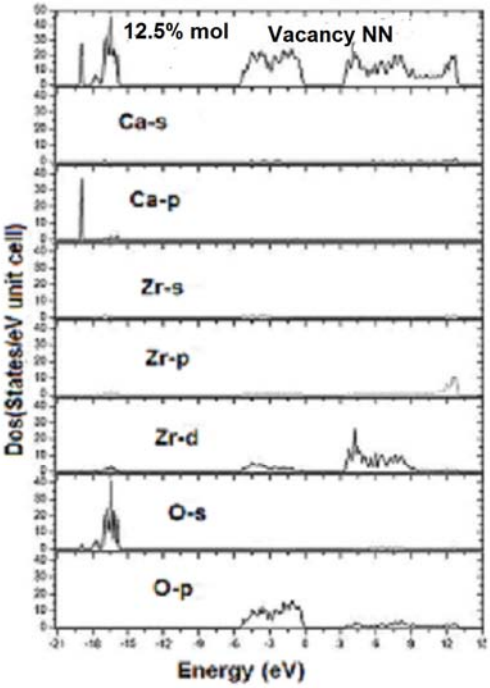

(E)

Fig. (14). contd….

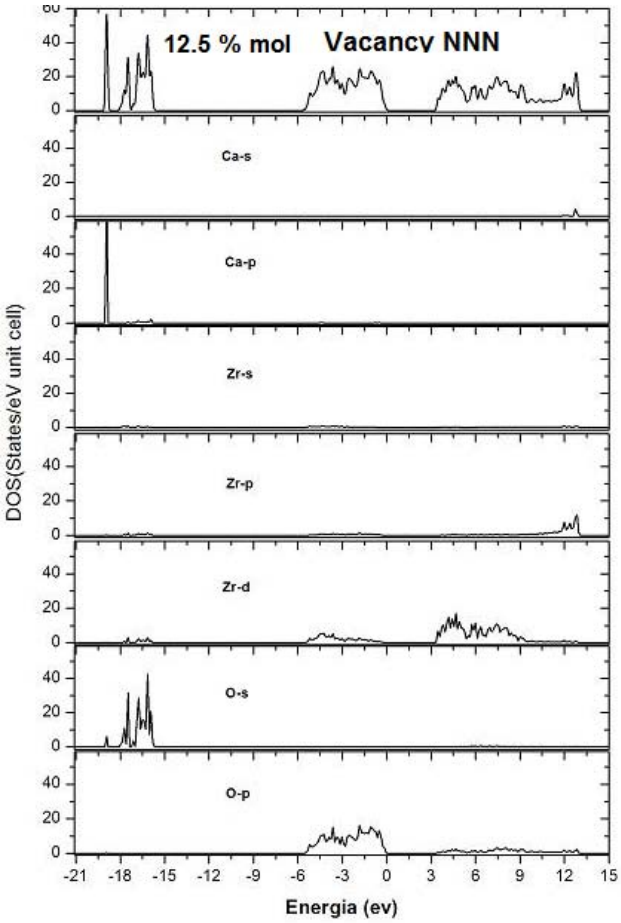

(F)

Fig. (14). (**a**) Total density of states for 25% mol CaO. (**b**) Total density of states for 12.5% mol CaO containing NN oxygen vacancies. (**c**) Total density of states for 12.5% mol CaO containing NNN oxygen vacancies. (**d**) Partial density of states per orbital for 25% mol CaO. (**e**) Partial density of states per orbital for 12.5% mol CaO containing Ca dopants and NN vacancies. (**f**) Total density of states per orbital for 12.5 % mol containing Ca dopants and NNN oxygen vacancies.

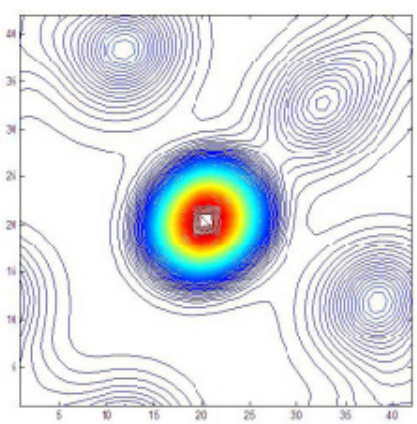

(A)

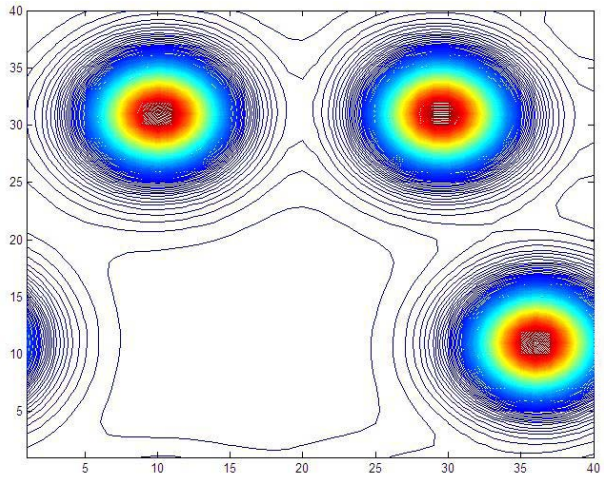

(B)

Fig. (15). contd….

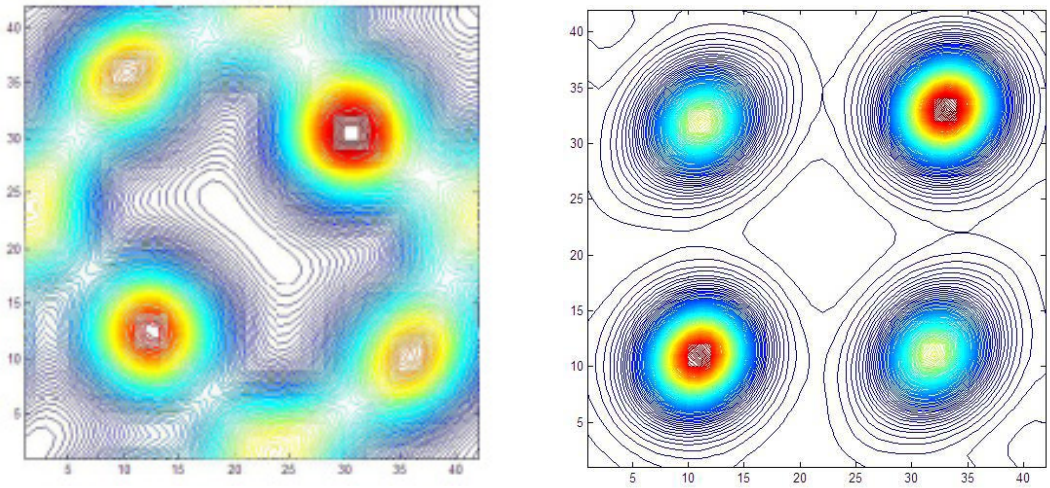

(C) **(D)**

Fig. (15). Density of charge in the direction (001) of the unit cell with 25% mol CaO. (**a**) Ca dopant. (**b**) Oxygen vacancies and atoms. (**c**) Oxygen and Zr. (**d**) Oxygens.

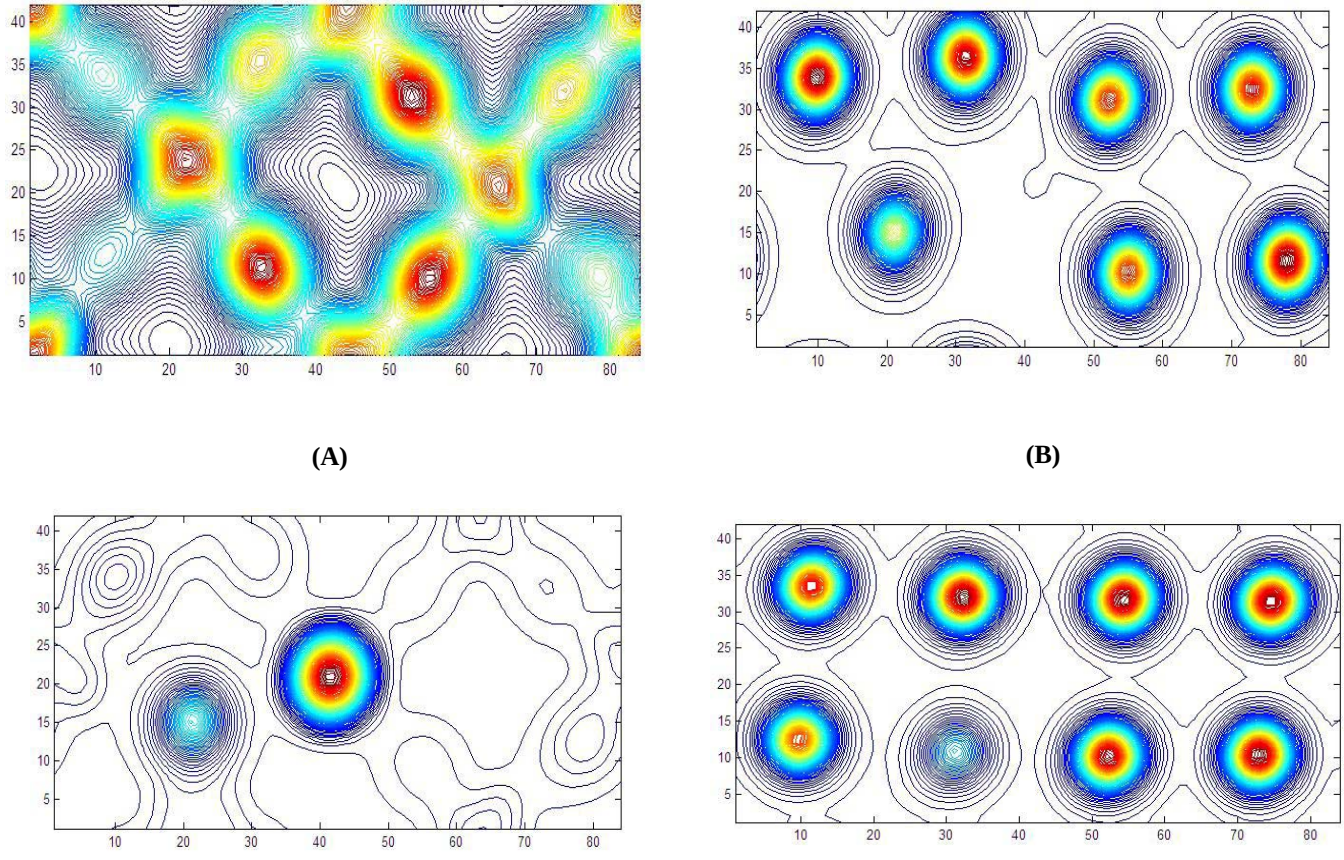

(A) **(B)**

(C) **(D)**

Fig. (16). Density of charge in the direction (001) of the unit cell with 12.5% CaO containing NN. (**a**) Zr. (**b**) Oxygen vacancies and atoms. (**c**) Calcium dopant. (**d**) Oxygens.

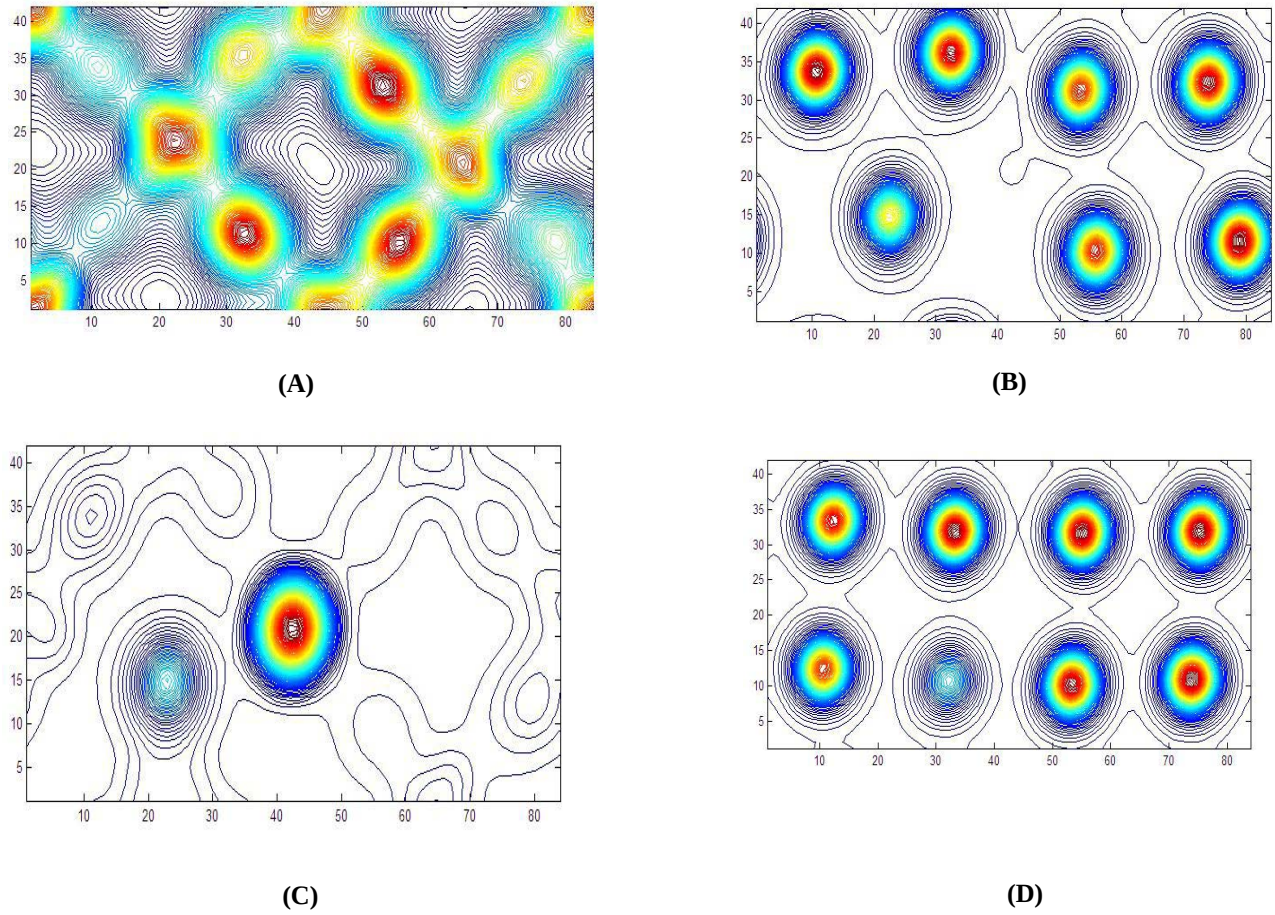

Fig. (17). Density of charge in the direction (001) of the unit cell 25% mol CaO containing containing NN oxygen vacancies. (**a**) Zr. (**b**) Oxygen vacancies and oxygens. (**c**) Dopant Ca and vacancy. (**d**) Oxygens.

layer where we find Zr. Fig. (**17b**) indicates the oxygen vacancy and new arrangement of oxygens, Fig. (**17c**) indicates the layer where we find dopant Ca. Fig. (**17d**) indicates the new arrangements of the oxygens. Covalent Zr-O bonds, ionic CaO bonds, oxygen migration (ionic conductivity) is suggested.

We show in Fig. (**18a** and **b**) ZrO_2 doped with trivalent cations. such as Sc^{3+}, i.e., ZrO_2-Sc_2O_3 solid solutions using concentration of 14.2 and 33% mol. The Sc^{3+} dopants as well as oxygen vacancies NN and NNN neighbors to dopants are explicity shown. Calculations were made to find the kinetic energies of cut (E_{cutoff}) as well as the number of k-points to obtain converged results.

The addition of impurities such as Ca^2, Mg^2, Y^3, Sc^3 with origin in the solid solution of Zirconia with oxides such as CaO, MgO and Y_2O_3, Sc_2O_3 does not favor the monoclinic phase m-ZrO_2, stabilizing the more symmetric phases which highly increases very much the thermodynamic properties of ZrO_2 allowing thus the production of materials with great resistance, hardness and resistance to thermal changes. With the increase of concentration of dopants the material transforms into a tetragonal phase called partially stabilized. With a larger amount of dopant material transforms to a cubic form called completely stabilized.

The dopant cations substitute the Zr^{4+} in the sublattice of cations forming by electrostatic compensation a vacancy of oxygen for each two Sc^3. In the case of Ca^2 a vacancy of oxygen is generated for each substitutional Ca. This simultaneous presence of dopant cations and oxygen vacancies in good concentration means that the whole environment is different from the stoichiometric pure zirconia phases (t and c-ZrO_2). A simple notion of this process of stabilization is attributed to the covalent bond of Zr-O which favors the coordination 7 as in the monoclinic phases. Thus the presence of oxygen vacancies in the stabilized zirconia system reduces the number of coordination from 8 as in the fluorite phase to a value near seven. In the case of addition of ions such as Ca^2. Doping with smaller metal ions do not force oxygens apart leaving the metals in seven fold coordination.

We give in Fig. (**19a**, **b**) total density of states for 33.3%, 14.2% mol Sc_2O_3 solid solution of Sc_2O_3-ZrO_2. In Fig. (**18a**) we include NNN oxygen vacancy with respect to Sc dopant. In Fig. (**18b**) we include both NN and NNN oxygen

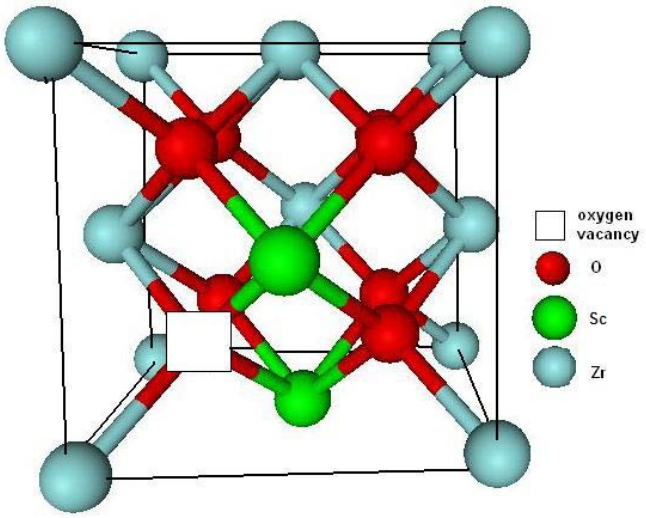

(a)

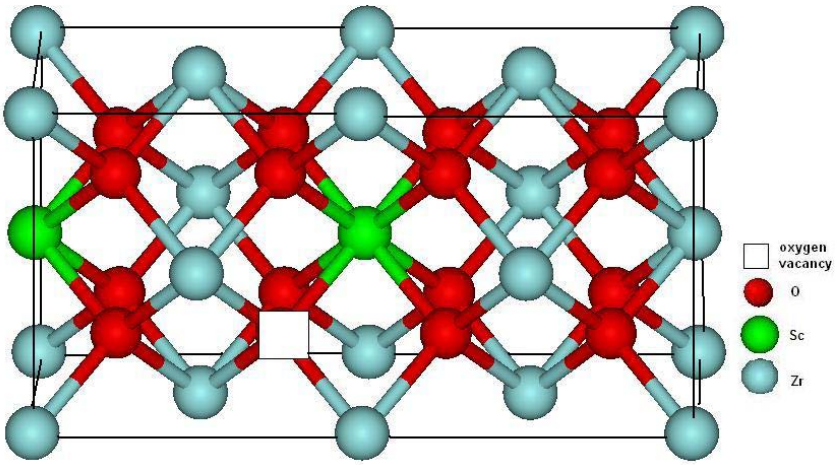

(b)

Fig. (18). Indicates unit cells for the solid solutions. (**a**) with 33% mol Sc_2O_3 and (**b**) with 14.2% mol Sc_2O_3 where □ indicates the oxygen vacancy with respect to the Sc atom dopant position.

vacancies with respect to dopant. We show in Figs. (**19c**), partial density of states per orbital for 33.3 and 14.2 % mol of Sc_2O_3. In the case of doping with trivalent ions, such as Sc^{3+} the deeper density of states are occupied by orbitals of the type Sc-p. In the valence bands the O-2s form part of the valence band whereas the top of the valence band is formed by O-2p orbitals. The conduction band is formed by orbitals of Zr and Sc with d character. There exist some charge transfer from the orbitals of the 0-p band of valence to the Zr-4d orbitals of the conduction band as can be observed.

We also determined the energetic jump (E_{gap}) between the occupied and virtual states for each composition. In the case of doping with Sc with a concentration of 33% mol we observe a large reduction of the gap form the bulk values of 3.03 eV to a value of 1.751 eV. In the case of concentration of dopants of 14.2% reduction is less radical with a gap value of 2.697 eV. It is known that for certain large concentrations of Sc the ionic conductivity is degraded. Sc_2O_3 stabillized Zirconia exhibits the highest conductivity in the zirconia solid solutions. Physical and chemical properties associated with these characteristics are closely related to the crystal structures and phase changes.

In Fig. (**20**) we show the density of charge in the direction (001) of the unit cell with 14.2 and 33.3 % mol Sc_2O_3 concentration respectively. Fig. (**20a**) indicating that the layer where the Zr and Sc are found. Fig. (**20b**) shows the oxygen vacancy and the new type of oxygen arrangement, Fig. (**20c**) indicates the layer for Sc dopants, Fig. (**20d**) indicates oxygen rearrangement. The vacancies and not too large dopants to allow rearrangements, relaxations, migration (ionic conductivity).

In Fig. (**21**) we show the charge density in the 100 direction for 14.2 % mol Sc2O3 %. Fig. (**21a**) shows Zr and oxygens, Fig. (**21b**) indicates oxygen vacancy and rearrangement, Fig. (**21c**) indicates Sc dopants. We observe Zr-O bonding, vacancies cause rearrangement, migrations,

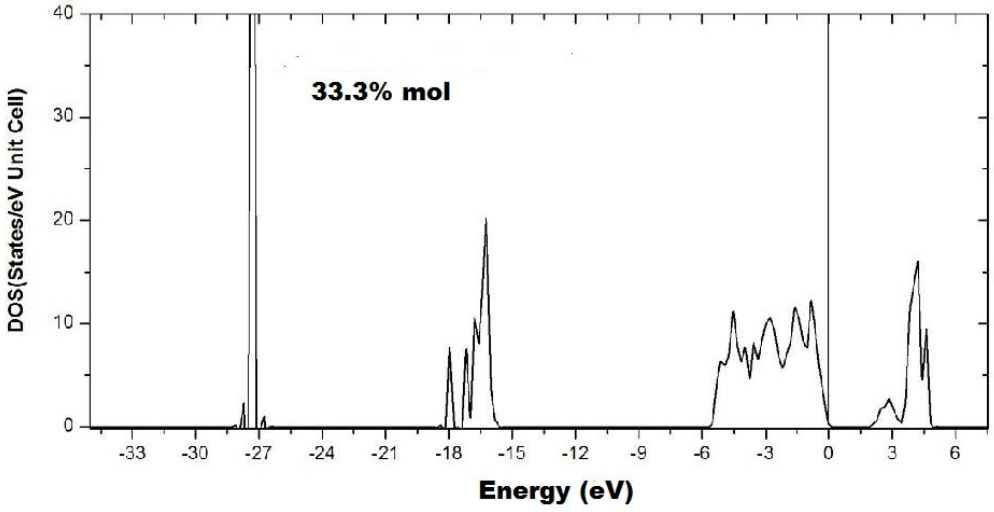

·(A)

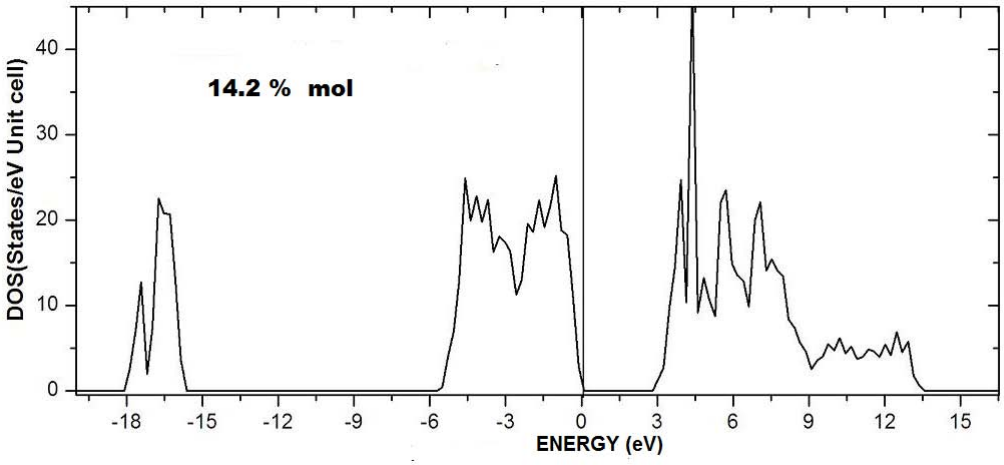

(B)

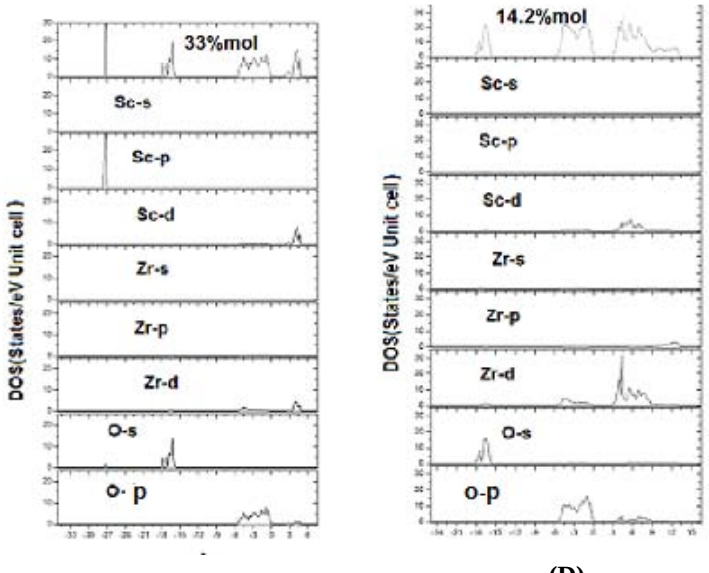

(C) **(D)**

Fig. (19). Density of state for. (**a**) 33% mol Sc_2O_3. (**b**) 14.2 % mol Sc_2O_3 with NN vacancy respect to Sc

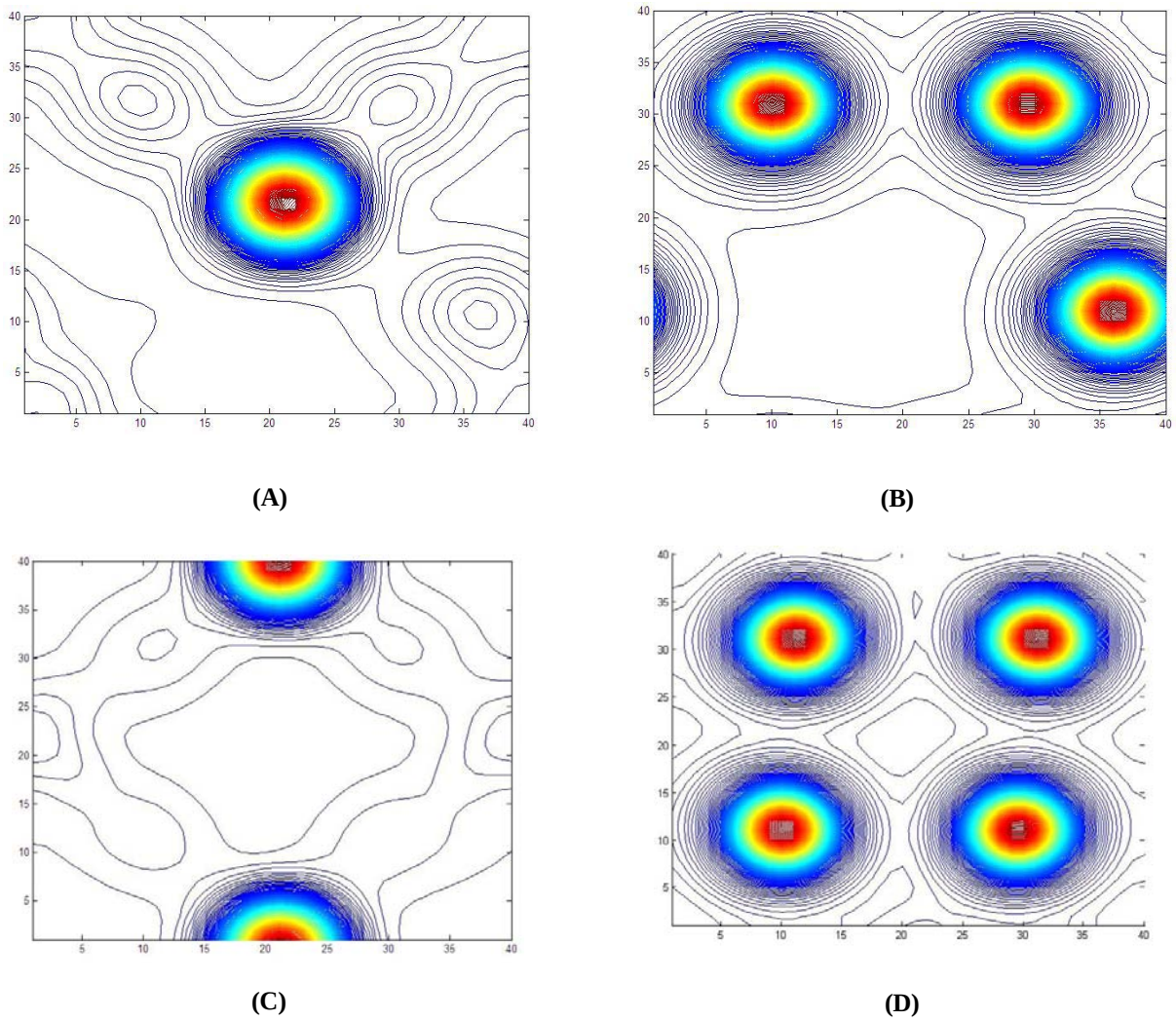

Fig. (20). Density of charge in the direction (001) of the unit cell 33.3 % mol Sc_2O_3. (**a**) Zr and Sc. (**b**) Vacancy and oxygens. (**c**) Dopants. (**d**) Oxygens.

conductivity of oxygens. The Sc also participates in bonding process which would lead to reduction of Zr coordination number.

Classical arguments [26] for ordering/disordering of cations and anions reference several driving forces: electrostatic interactions, coordination preference and elastic strain. The electrostatic interaction of vacancies with cations suggests that positively charged vacancies would associate more closely with lower valent Sc^{3+}, Ca^{2+} than Zr^{4+}. A coordination driven argument suggest that vacancies in stabilized Zr would associate with Zr rather than or Sc^{3+} to decrease the Zr coordination from eight to seven. Elastic strain could also influence ordering. The differences in sizes of the cations may create strain fields around the larger ions. The presence of a vacancy, in addition, creates a large physical distortion. In addition, relaxations and displacements of ions from cubic fluorite sites, vacancy positions relative to zirconium and dopant positions, microscopic order of ion aggregates and effects of cation arrangement on oxygen diffusion can be important. The role of the dopant should increase as it`s concentration increases and it's size and charge changes. As the number of vacancies increases with doping, the conductivity increases until the number of large dopant-dopant edges inhibit oxygen diffusion. Factors for stabilized zirconia at different temperatures include hybridization, density of states, diffusion of oxygen to vacant sites, distribution of vacancies, vacancy ordering, coordination of Zr, dopant, oxygen and vacancies, chain of vacancies, relaxation with dopant concentration, relaxation of cations around dopants and Zr, vacancy position relative to dopant and Zr. The precise contribution of each of the driving forces to atomic arrangements that takes us closer to lower temperature stabilized materials is important.

Our results suggest that bonding, hybridization, charge transfer, migration, relaxation, reorganization, ionic conductivity caused by presence of dopants with different

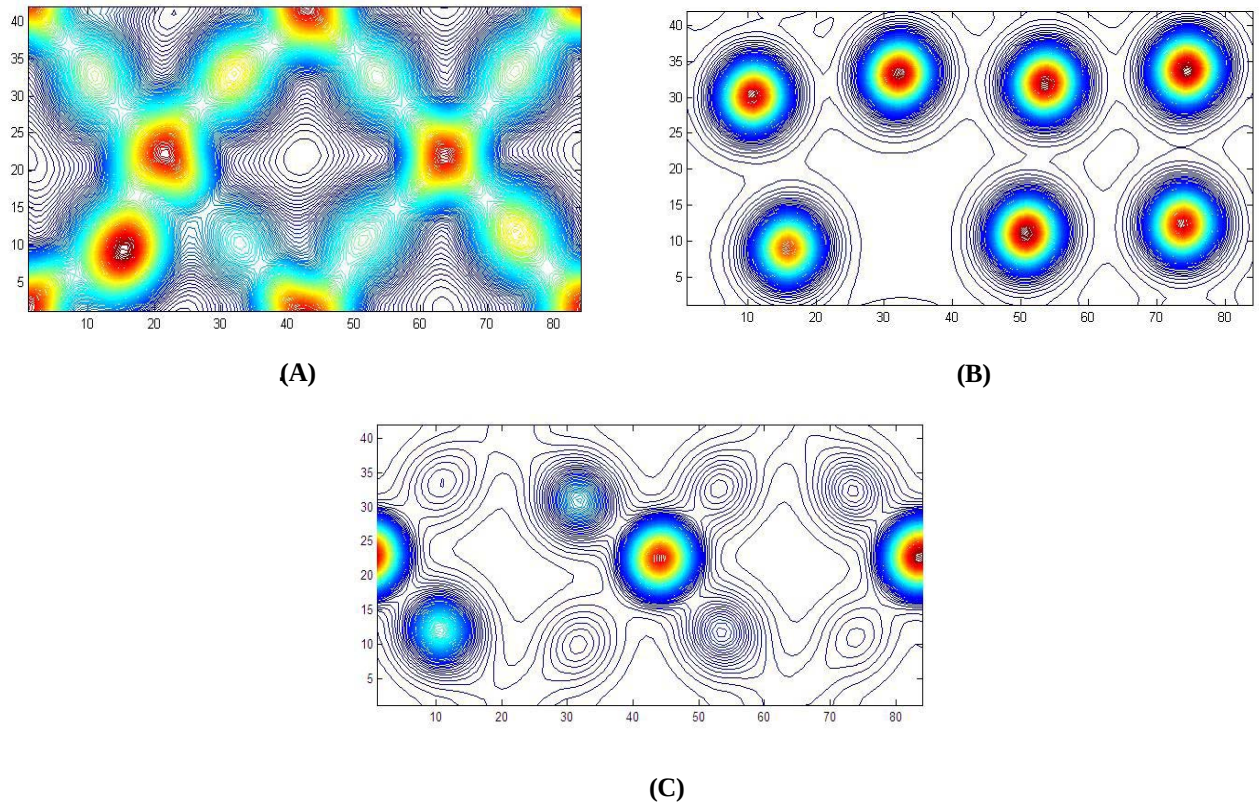

Fig. (21). Density of charge in the direction (001) of the unit cell with 14.2 % mol Sc_2O_3 containing NN vacancy. (**a**) Zr. (**b**) Oxygen vacancy and oxygens. (**c**) Sc dopant.

charges, sizes, concentrations as well as vacancies will yield electrolytes with different properties, some of which will be ideal for SOFCs applications.

We observe an electrostatic Zr-O covalent bonding in all cases. Dopants should be NNN to vacancies in order to assist in lowering coordination of Zr and not hinder ionic migration (oxygen mobility). Methods of synthesis and differing temperature annealing can be influential since defect formation is at the root of the technology. Doping fluorite-structured zirconia with aliovalent cations increases the number of charge-compensating oxygen vacancies which are directly responsible for the ionic conduction in the system. Dopant size and charge are also important, i.e we note that trivalent cation Sc with similar radius of Zr has the highest ionic conductivity whereas divalent Ca with a smaller charge has a dipole/tripole ratio more favorable for ionic conductivity with increased doping.

From the basic notions and first principles derived knowledge it becomes clear that if we use the properly modified material we solve the problem. Are we using `nanotechnology` to mount the atoms one by one` in the positions that would give the materials the exact properties we are searching for?

CONCLUSIONS

Our results indicate strong driving forces due to hybridization between Zr(4d) and O(2p). The characterisics of the materials (dopant, vacancies, defects, concentrations) can modify the electrolyte parameters towards a system which is an ionic conductor without being an electronic conductor and operate at lower temperatures. The manner of synthesis is also important. There is a lot of new work reported, i.e using in general different materials which always however have some limitations to make the electrolyte stable at lower temperatures and commercially viable. It is our belief however that with nanotechnology we will soon be able to mount the atoms one by one in the right places to make this technology work.

CONFLICT OF INTEREST

The author(s) confirm that this article content has no conflict of interest.

ACKNOWLEDGEMENTS

We acknowledge financial support from CNPq, Faperj.

REFERENCES

[1] Huang, J.; Xie, F.; Wang, C.; Mao, Z. Development of solid oxide fuel cell materials for intermediate-to-low temperature operation. *Int. J. Hydrogen Energ.*, **2012**, *37*, 877-883.

[2] Fabbri, E.; Bi, L.; Pergolesi, D.; Traversa, E. Towards the next generation of solid oxide fuel cells operating below 600 ^{o}C with chemically stable proton-conducting electrolytes. *Adv. Mater.*, **2012**, *24*, 195-208.

[3] Shimazu, M.; Isobe, T.; Ando, S.; Hiwatashi, K.; Ueno, A.; Yamaji, K.; Kishimoto, H.; Yokokawa, H.; Nakajima, A.; Okada, K. Stability of Sc_2O_3 and CeO_2 CO-doped ZrO_2 Electrolyte during the Operation of Solid Oxide Fuel Cells. *Solid State Ionics*, **2011**, *182*, 120-126.

[4] Merle, G.; Wessling, M.; Nijmeijer, K. Anion exchange membranes for alkaline fuel cells: A review. *J. Membrane. Sci.*, **2011**, *377*, 1-35.

[5] Bessler, W.G.; Vogler, M.; Stormer, H.; Gerthsen, D.; Utz, A.; Weberd, A.; and Ivers-Tiffe, E. Model anodes and anode models for understanding the mechanism of hydrogen oxidation in solid oxide fuel cells. *Phys. Chem. Chem. Phys.*, **2010**, *12*, 13888-13903.

[6] Rand, D.A.J.; Dell, R.M. Hydrogen Energy: Challenge and Prospects. *J. Appl. Electrochem.*, **2009**, *39*, 311-312.

[7] Suna, C.; Stimming, U.; Recent anode advances in solid oxide fuel cells. *J. Power Sources*, **2007**, *171*, 247-260.

[8] Singhal, S.C. and K. Kendall, K. High-temperature solid oxide fuel cells: Fundamentals, design and applications, *Elsevier Science*, Oxford, **2003**.

[9] Moure, C.; Gutierrez, D.; Tartaj, J.; Capel, F.; Duran, P. Chemical and electrical features of the interphase: electrode-electrolyte in the system $(Y,Ca)/MnO_3$ $-CeO_2$ $-Y_2O_3$. *Solid State Ionics*, **2001**, *141*, 381-386.

[10] Fabbri, E.; Bi, L.; Pergolesi, D.; Traversa, E. Towards the Next Generation of Solid Oxide Fuel Cells Operating Below 600 °C with Chemically Stable Proton-Conducting Electrolytes. *Adv. Mater.*, **2012**, *24*, 195-208

[11] Steele, B.C.H.; Heinzel, A. Materials for fuel-cell technologies. *Nature*, **2001**, *414*, 345-352.

[12] Liu, Q.J; Liu, Z.T.; Feng, L.P. Elasticity, electronic structure, chemical bonding and optical properties of monoclinic ZrO_2 from first-principles. *Physica. B.*, **2011**, *406*, 345-350.

[13] Ren, H.S.; Zhu, B.; Zhu, J.; Hao, Y.; Yu, B.; Li, Y. The structural phase transition and elastic properties of zirconia under high pressure from first-principles calculations. *Solid State Sci.*, **2011**, *13*, 938-943.

[14] Koirala, R.; Krishna, R.; Gunugunuri, S.E.P.; Smirniotis, P.G.S. Effect of Zirconia Doping on the Structure and Stability of CaO-Based Sorbents for CO_2 Capture during Extended Operating Cycles. *J. Phys. Chem. C.*, **2011**, *115*, 24804-24812

[15] Aldebert, P.; Traverse, J.P. Structure and Ionic Mobility of Zirconia at High Temperature. *J. Am. Ceram. Soc.*, **1985**, *68*, 34-40.

[16] Hafner, J. Ab-Initio Simulations of Materials Using VASP: Density-Functional Theory and Beyond. *J. Comput. Chem.*, **2008**, *29*, 2044-2078.

[17] Parr, R.; Yang, W. Density functional theory of atoms and molecules, Oxford Science Publications (**1994**).

[18] Blöchl, P.E. Projector augmented-wave method. *Phys. Rev. B.*, **1994**, *50*, 17953-17979.

[19] Kresse, G.; Furthmüller, J. Efficiency of ab-initio total energy calculations for metals and semiconductors using a plane-wave basis set. *Comput. Mat. Sci.*, **1996**, *6*, 15-50.

[20] Kresse, G.; Furthmüller, J. Efficient iterative schemes for ab initio total-energy calculations using a plane-wave basis set. *Phys. Rev. B.*, **1996**, *54*, 11169-11186.

[21] Kresse, G.; and Hafner, J. Ab-initio Molecular-dynamics for open-shell transition-metals. *Phys. Rev. B.*, **1993**, *48*, 13115-13118.

[22] Kresse, G. and Hafner, J. Norm-conserving and ultrasolft pseudo-potentials for first-row transition elements. *J. Phys. Condens. Matter*, **1994**, *6*, 8245.

[23] Available online at httl://cms.mpi.univie.ac.at/vasp/

[24] Abufager, P.N.; Canchaya, J.G.S.; Wang, Y.; Alcam , M.; Martín, F.; Soria, L.A.; Martiarena, M.L.; Reuter, K.; Busnengo, H.F. Theoretical study of the structure of self-assembled monolayers of short alkylthiolates on Au(111) and Ag(111): the role of induced substrate reconstruction and chain-chain interactions. *Phys. Chem. Chem. Phys.*, **2011**, *13*, 9353-9362.

[25] Canchaya, J.G. Solano; Wang, Y.; Alcamí, M.; Martín, F.; Busnengo, H.F. Study of the interaction between short alkanethiols from ab initio calculations. *Phys. Chem. Chem. Phys.*, **2010**, *12*, 7555-7565.

[26] Predith, A.P. Computational studies of cation and anion ordering in cubic Yttria Stabilized Zirconia, Phd. Thesis, MIT, Dept. of Mat. Science and Engineering (**2006**).

[27] McComb, D.W. Bonding and electronic structure in zirconia pseudopolymorphs investigated by electron energy-loss spectroscopy. *Phys. Rev. B.*, **1996**, *54*, 7094-7102.

[28] Ganduglia-Pirovano, M.G.; Hoffmann, A.; Sauer, J. Oxygen vacancies in transition metal and rare earth oxides: Current state of understanding and remaining challenges. *J. Surf. Sci. Rep.*, **2007**, *62*, 219-270.

[29] French, R.H.; Glass, S.J.; Ohuchi, F.; Xu, Y.N.; Ching, W.Y. Experimental and theoretical determination of the electronic structure and optical properties of three phases of ZrO_2. *Phys. Rev. B.*, **1994**, *49*, 5133-5141.

[30] Xiong, K.; Robertson, J.; Gibson, M.C.; Clark, S.J. Defect energy levels in HfO_2 high-dielectric-constant gate oxide. *Appl. Phys. Lett.*, **2005**, *87*, 183505-183508.

[31] Broqvist, P.; Alkauskas, A.; Pasquarello, A. Band alignments and defect levels in Si-HfO2 gate stacks: Oxygen vacancy and Fermi-level pinning. *Appl. Phys. Lett.*, **2008**, *92*, 132911-132914.

[32] Broqvist, P.; Pasquarello, A. Oxygen vacancy in monoclinic HfO_2: A consistent interpretation of trap assisted conduction, direct electron injection and optical absorption experiments. *Appl. Phys. Lett.*, **2006**, *89*, 262904-262907.

[33] Kralik, B.; Chang, E.K.; Louie, S.G. Structural properties and quasiparticle band structure of zirconia. *Phys. Rev. B.*, **1998**, *57*, 7027-7036.

Received: January 06, 2012 **Revised: July 25, 2012** **Accepted: July 31, 2012**